Activating killer cell immunoglobulin-like receptor 2DS2 binds to HLA-A*11

Jingxian Liu[a], Ziwei Xiao[a], Hui Ling Ko[a], Meixin Shen[a], and Ee Chee Ren[a,b,1]

[a]Singapore Immunology Network, Agency for Science, Technology and Research, Singapore 138648; and [b]Department of Microbiology, Yong Loo Lin School of Medicine, National University of Singapore, Singapore 117597

Edited by Wayne M. Yokoyama, Washington University School of Medicine, St. Louis, MO, and approved January 8, 2014 (received for review November 26, 2013)

Inhibitory killer cell Ig-like receptors (KIRs) are known to recognize HLA ligands mainly of the HLA-C and Bw4 groups, but the ligands for KIRs are poorly understood. We report here the identification of the cognate ligand for the activating KIR 2DS2 as HLA-A*11:01. The crystal structure of the KIR2DS2–HLA-A*11:01 complex was solved at 2.5-Å resolution and revealed residue-binding characteristics distinct from those of inhibitory KIRs with HLA-C and the critical role of residues Tyr45 and Asp72 in shaping binding specificity to HLA-A*11:01. Using KIR2DS2 tetramers, binding to surface HLA-A*11:01 on live cells was demonstrated and, furthermore, that binding can be altered by residue changes at p8 of the peptide, indicating the influence of peptide sequence on KIR–HLA association. In addition, heteronuclear single quantum coherence NMR was used to map the involvement of critical residues in HLA binding at the interface of KIR and HLA, and validates the data observed in the crystal structure. Our data provide structural evidence of the recognition of A*11:01 by the activating KIR2DS2 and extend our understanding of the KIR–HLA binding spectrum.

Human killer cell Ig-like receptors (KIRs) are transmembrane glycoproteins expressed on natural killer (NK) cells that detect the expression levels of major histocompatibility complex (MHC) class I on normal and diseased cells (1–3). In humans, *KIR* genes are divided into inhibitory type (2DL and 3DL) and activating type (2DS, 3DS, and 2DL4), which are receptors with two or three C2-type Ig-like extracellular domains (4–6). Whereas the human leukocyte antigen (HLA)-ligand specificities for inhibitory KIRs are relatively well studied, with available structural information for three KIR-DL–HLA complexes, the ligands for activating KIRs are not well-defined and no KIR-DS–HLA complexes have been described (7, 8). We report here the structure of the activating KIR2DS2 in complex with HLA-A*11:01 and a vaccinia viral peptide. The solved structure at 2.5-Å resolution reveals that Tyr45, which is a residue specific to KIR2DS2, forms a hydrogen bond with the backbone of the HLA α1-helix at Thr80 and contributes to the binding specificity of KIR2DS2–A*11:01. This is a distinct departure from the inhibitory KIRs that use position 44, which engages the dimorphic HLA-C1 (Asn80) or HLA-C2 (Lys80) epitope of HLA-C. These data provide a detailed description of the unique features that characterize the binding of an activating KIR and its cognate HLA ligand.

Results

Crystal Structure of the KIR2DS2–HLA-A*11:01 Complex. Human KIRs have been reported to bind HLAs that carry a selective range of epitopes including C1, C2, Bw4, and A3/A11 (1, 9). Crystal structures of KIR2DL1–C*04:01 (10), KIR2DL2–C*03:04 (11), and KIR3DL1–B*57:01 (12) in complex with their respective HLA ligands are available, but there is as yet none for activating KIRs. The activating KIR 2DS2 is an interesting KIR that has been associated with NK responses and susceptibility to cytomegalovirus (13), hepatitis C virus (14), and ulcerative colitis (15). It has very close sequence similarity to KIR2DL2 and KIR2DL3, differing only in four and two amino acid residues, respectively, and, despite having only these few substitutions, binding to HLA-C was abrogated (16, 17). KIR, HLA, and β_2-microglobulin recombinant proteins were refolded (18), and cocrystals of KIR2DS2–*001 and –A*11:01 bound to the vaccinia virion membrane protein A14-derived peptide MLIYSMWGK (Immune Epitope Database and Analysis Resource, Epitope ID 41975; www.iedb.org/assay_details.php?assayId=1359384) were successfully generated and its structure was determined to 2.5-Å resolution (Fig. 1 *A* and *B* and Table 1). The molecular packing resulted in two KIR2DS2–HLA-A*11:01 complexes in one asymmetric unit in a "head-to-tail" arrangement, and contact with the complex can be observed between the D2 domain of KIR2DS2 and N terminus of the peptide-binding grove of the heavy chain (Fig. S1 *A* and *B* and Table S1). KIR2DS2 bound to HLA-A*11:01 consists of two C2-type Ig-like domains termed D1 and D2, and displays a root-mean-square deviation (rmsd for 192 paired Cα) of 2.16 Å with free 2DS2 (19), 1.17 Å with KIR2DL1–C*04:01, and 0.97 Å with KIR2DL2–C*03:04. The total buried surface area between the D1 and D2 domains is 1,020 Å^2, which is similar to the reported values for inhibitory KIRs of 2DL1 (1,076 Å^2), 2DL3 (1,050 Å^2), and 2DL2 (919 Å^2). The interface between HLA-A*11:01 and KIR2DS2 is 1,180 Å^2, which is the smallest among KIR–HLA complexes of KIR2DL1–C*04:01 (1,485 Å^2), KIR2DL2–C*03:04 (1,562 Å^2), and KIR3DL1–B*57:01 (1,740 Å^2). Comparing the hinge angle of the free KIR2DS2 (19) with that of the

Significance

Killer cell immunoglobulin-like receptors (KIRs) function as key recognition elements in innate immunity. Structural information for inhibitory KIRs 2DL2, 2DL1, and 3DL1 in complex with their respective HLA ligands is available, but such data for activating KIRs are lacking. We report here the successful crystallization and solved structure of the activating KIR2DS2 in complex with HLA-A*11:01. The structure clearly explains the role of Tyr45, which has long puzzled KIR researchers because it differentiates KIR2DS2 from all inhibitory KIRs, and is now shown to bind Thr80 of HLA-A*11:01. Using KIR2DS2 tetramers to bind HLA on live cells, we also provide evidence that peptide sequence can affect KIR–HLA binding. Our data thus resolve a long-standing problem in KIR biology.

Author contributions: J.L. and E.C.R. designed research; J.L. performed crystallographic preparation, solved structure, and analyzed NMR data; J.L. and Z.X. performed surface plasmon resonance assay; J.L., Z.X., H.L.K., and M.S. contributed new reagents/analytic tools; J.L. and E.C.R. analyzed data; and J.L. and E.C.R. wrote the paper.

The authors declare no conflict of interest.

This article is a PNAS Direct Submission.

Data deposition: Crystallography, atomic coordinates, and structure factors reported in this paper have been deposited in the Protein Data Bank, www.pdb.org (PDB ID code 4N8V).

[1]To whom correspondence should be addressed. E-mail: ren_ee_chee@immunol.a-star.edu.sg.

This article contains supporting information online at www.pnas.org/lookup/suppl/doi:10.1073/pnas.1322052111/-/DCSupplemental.

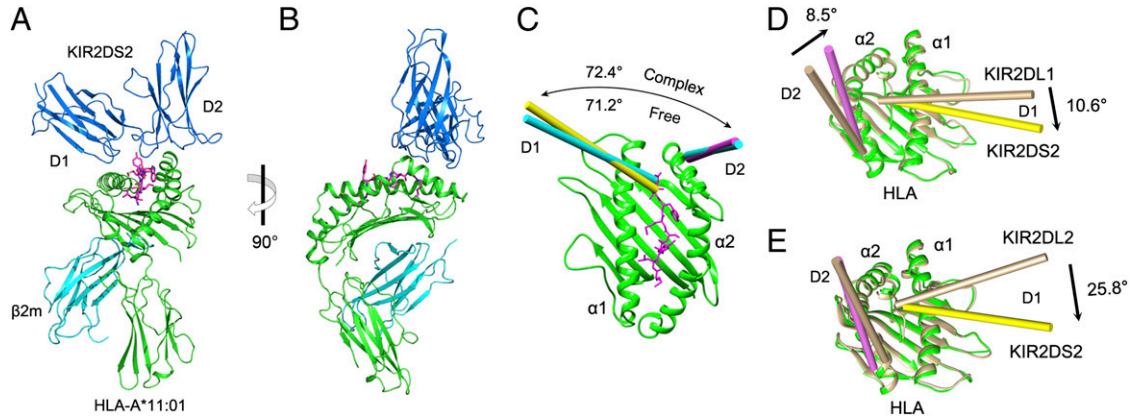

Fig. 1. Structure of the KIR2DS2*001–HLA-A*11:01 complex and hinge angle comparison. (*A* and *B*) Orthogonal views of the crystal structure of the KIR–HLA complex. KIR2DS2*001, HLA, β_2-microglobulin (β2m), and peptide are colored marine blue, green, cyan, and violet, respectively. (*C*) Comparison of hinge angle of KIR2DS2 in ternary complex (with HLA) versus free (without HLA). Domain axes angles between KIR2DS2 and KIR2DL1 or KIR2DL2 after structure alignment of HLA molecules in KIR–HLA complexes: (*D*) A 10.6° D1 domain axis angle and 8.5° D2 domain axis angle between KIR2DS2 (yellow, violet) and KIR2DL1 (wheat, brown); (*E*) A 25.8° axis angle for the D1 domain between KIR2DS2 (yellow) and KIR2DL2 (wheat).

complexed KIR2DS2, there is only a small expansion of the hinge angle induced by the binding from 71.2° to 72.4° (Fig. 1*C*). However, after superimposing HLA molecules of different HLA–KIR complexes, the relative orientations of the D1 and D2 domains displayed significant differences. The D1 and D2 domain axes of KIR2DS2–HLA-A*11:01 differ from those of KIR2DL1–HLA-C*04:01 by 10.6° and 8.5°, respectively (Fig. 1*D*). A more significant D1 axis difference of 25.8° was observed between KIR2DS2–HLA-A*11:01 and KIR2DL2–HLA-C*03:04, whereas the D2 axis remained similar. The consequence of this D1 orientation in KIR2DS2 results in the shift of the CC′ loop toward the C-terminal region of the HLA α1-helix. The CC′ loop of the D1 domain, hinge region, and BC and FG loops in the D2 domain of KIR2DS2 are the main contact points with the HLA α1- and α2-helical regions (Fig. 2 *A* and *B* and Fig. S2). The CC′ loop of KIR2DS2 was observed to be positioned more toward the C terminus of the α1-helix of HLA-A*11:01, and this displacement was 2.6 Å compared with KIR2DL1 (Fig. 2*A*) and an even more significant difference of 6.2 Å compared with KIR2DL2 (Fig. 2*B*). In KIR2DL2, residue Phe45 located at the tip of the CC′ loop is inserted into the groove of the α1-helix of HLA residues 75–80 and is surrounded by atoms through hydrophobic interactions (Fig. 2*C*). However, Tyr45 of KIR2DS2 shifts toward the C terminus of the α1-helix, allowing it to contact the NH group of HLA Thr80 to form a hydrogen bond (Fig. 2*C*).

Table 1. Data collection and refinement statistics

	KIR2DS2-HLA-A*11:01
Data collection	
Space group	$P2_12_12_1$
Molecules, AU	2
Cell dimensions	
a, *b*, *c*, Å	69.5, 94.7, 228.4
α, β, γ, °	90.0, 90.0, 90.0
Wavelength, Å	0.999969
Resolution range, Å	66.53–2.50 (2.63–2.50)
R_{merge}*	0.17 (0.58)
$I/\sigma(I)$	7.5 (2.4)
Completeness, %	99.5 (99.9)
Redundancy	7.4 (7.4)
Unique reflections	52,897 (7,618)
Refinement	
Resolution, Å	2.50 (2.59–2.50)
No. of reflections	52,797 (5,201)
R_{work}/R_{free}†	0.222/0.257
No. of atoms	9,364
Protein	9,240
Water	124
Protein residues	1,145
B factors, Å^2	
Protein	37.10
Solvent	30.10
Rms deviations	
Bond lengths, Å	0.008
Bond angles, °	1.13
Ramachandran plot, %	
Favored region	97.1
Allowed region	2.9
Disallowed region	0.0

Values in parentheses refer to the highest-resolution shell. AU, asymmetric unit.
*$R_{merge} = \Sigma_{hkl}\,\Sigma_i\,|I_i(hkl) - \langle I_i(hkl)\rangle|/\Sigma_{hkl}\,\Sigma_i\,I_i(hkl)$.
†R_{free} is the same as R_{cryst} and is calculated on 5% of the data excluded from refinement.

The conserved interdomain salt bridge Asp98-Arg149 present in all inhibitory KIR molecules is not observed in KIR2DS2. For inhibitory KIRs, this salt bridge is disrupted by conformational change when the KIR binds to HLA and contributes to the increase in the interdomain hinge angle of the complexed KIR2DL2. With KIR2DS2, the Nη1 and Nη2 groups of Arg149 are >8 Å away from the carboxyl groups of Asp98 in its free form and narrow slightly to 5.5 and 5.9 Å, respectively, after binding to HLA-A*11:01. Pro16 in the KIR2DS2 D1 domain, which in KIR2DL1/2DL2 is Arg16, lies at the interdomain interface, and this difference in side-chain volume may also contribute to the shaping of the hinge angle.

Shape complementarity for the interface of KIR2DS2 and HLA-A*11:01 showed a calculated mean value of shape correlation statistic of 0.64 and suggests that molecular bond formation contributes significantly to the binding interaction. Of these, the most important appears to be formation of salt bridges (KIR–HLA: Asp72-Arg75, Asp135-Arg145, Glu187-Lys146) and hydrogen bonds (KIR–HLA: Tyr45-Thr80, Glu106-Ala149, Ser133-Arg145, Ser184-Lys146). A comparison with the inhibitory KIR2DL1–HLA-C*04:01 and KIR2DL2–HLA-C*03:04 structures shows the use of Tyr45, Asp72, Tyr134, and Glu87 in KIR2DS2 to create new interactions that contribute to its binding specificity with A*11:01 (Table S2).

The footprint of the interaction on the A*11:01 surface shows the area on the α1-helix surface comprising Gln72, Arg75, Val76,

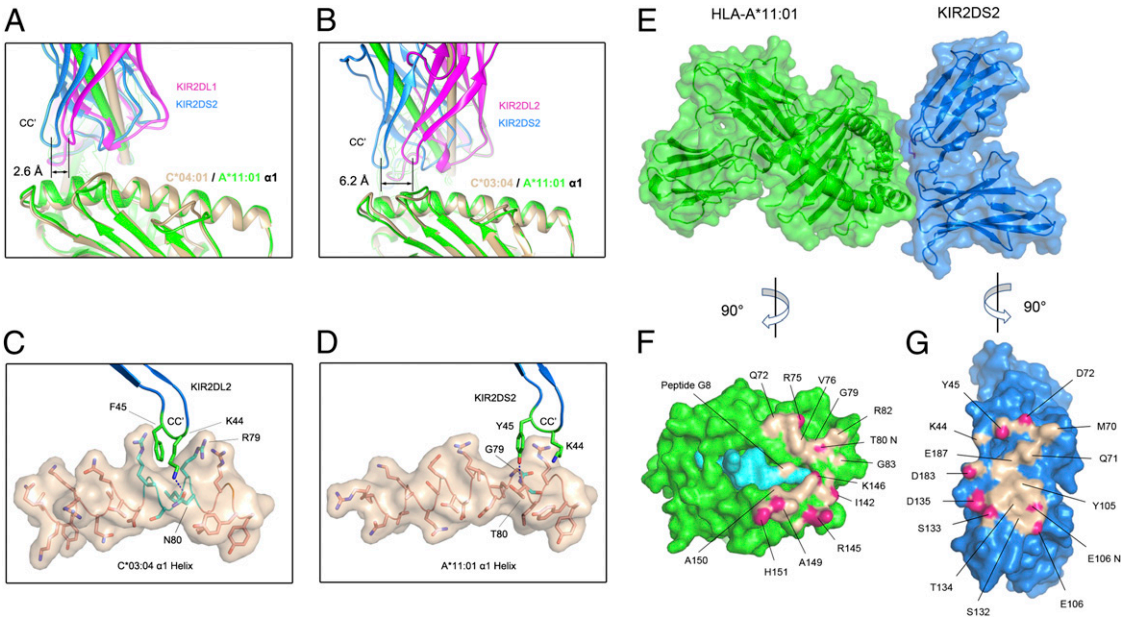

Fig. 2. CC′ loop displacement and footprint of the contact area. (*A*) Relative positions of the CC′ loop of KIR2DS2 (marine blue) and KIR2DL1 (violet). (*B*) Relative positions of the CC′ loop of KIR2DS2 (marine blue) and KIR2DL2 (violet). (*C*) F45 of KIR2DL2 inserts into the helix groove of HLA-C*03:04. The HLA α1-helix region 76–80 surrounding KIR2DS2 F45 is highlighted in cyan. (*D*) Y45 of KIR2DS2 contacts the backbone of HLA-A*11:01 at Thr80. Surface representation of HLA α1-helix 64–85 is shown in wheat. (*E*) Surface representation of KIR2DS2 (marine blue) and HLA-A*11:01 (green). (*F* and *G*) Contact area of KIR2DS2 and HLA-A*11:01. Contact areas within 3.4 Å are highlighted in pink; contact areas within 5 Å are highlighted in wheat.

Gly79, Thr80, Arg82, and Gly83 to make contact with D1 of KIR2DS2 (Fig. 2 *E*–*G*). Specifically, hydrogen bonds between the D1 domain and HLA α1-helix at Asp72-Arg75 and Tyr45-Thr80 were observed (Table S3). The D2 domain engages the HLA α2-helix across a larger number of residues including Ile142, Arg145, Lys146, Ala149, Ala150, and His151.

NMR Titration of the KIR–HLA Interaction. With the availability of the solved crystal structure, we sought to confirm these observations using an alternative approach, and examined the KIR2DS2–HLA-A*11:01 binding interactions using transverse relaxation-optimized spectroscopy-heteronuclear single quantum coherence (TROSY-HSQC), which is a highly sensitive method of assigning positions of specific atoms and determining chemical shifts indicative of binding interactions (Fig. 3 and Fig. S3). Tyr45 is unique to KIR2DS2, and it has been proposed that KIR2DS2 evolved away from binding the HLA-C1 epitope by substitution of Phe45 with Tyr45 (16, 17). The importance of position 45, illustrated by a swap from Tyr45 to Phe45, is sufficient to restore some binding (although not to the same degree as KIR2DL2) with the Lys80 C1 epitope (17). In the KIR2DS2–A*11:01 structure, the Tyr45 side chain orients toward the α1-helix and hydrogen-bonds with the Thr80 backbone NH group. NMR analysis showed a chemical shift change at Tyr45 when HLA-A*11:01 was titrated into the KIR2DS2 sample (Fig. 3*C′*), thus confirming its role in KIR2DS2 binding. An interesting feature to be tested is position 44 of KIR2DS2, which in inhibitory KIRs determines the dimorphic binding characteristic between the C1 and C2 epitopes of HLA-C (16, 20). From the NMR and structural data, Lys44 can be seen to have only a weak hydrophobic interaction with Ala83 (Fig. 3*B′*), and thus appears to have a diminished role in KIR2DS2 compared with the inhibitory KIRs.

KIR3DL2 and KIR2DS4 have been reported to bind A*11 and that Lys44, Pro71, and Val72 are important for this interaction (15, 16). Position 71 in KIR2DS2 is Gln71 and shows polar interaction with the Val76 backbone of A*11:01 (Fig. 3*D*). Similar to the structure of KIR2DL2–C*03:01, the tip of KIR2DS2 Gln71 interacts with p8 of peptide bound to HLA-A*11:01, indicating the potential role of peptide in recognition of HLA-A*11:01 by KIR2DS2. Only a slight chemical shift change was observed in the NMR titration experiment, which is consistent with an overall moderate binding interaction (Fig. 3*D′*). Asp72 of KIR2DS2 hydrogen-bonds with Arg75 of HLA-A*11:01 (Fig. 3*E*), and this KIR-HLA interaction has not been described previously in inhibitory KIR binding. The TROSY-HSQC spectrum detects a strong chemical shift signature for Asp72 and supports the nature of this binding interaction (Fig. 3*E′*).

The salt bridge Ser133/Asp135-Arg145 and hydrogen bond Glu106-Ala149/His151 (Fig. 3 *F*, *G*, *F′*, and *G′*) conserved in inhibitory KIRs can also be seen in KIR2DS2–HLA-A*11:01, and this represents the retained homology between KIR2DS2 and the inhibitory KIRs. Interestingly, a hydrogen bond that is usually formed between Asp183 of inhibitory KIRs and Lys146 of HLA is now made by Ser184 of KIR2DS2 (Fig. 3 *H* and *H′*). This slight change to accommodate a subtle shift in the FG loop preserves the hydrogen bond, which is important for maintaining the overall integrity of the KIR–HLA complex.

Tetramer Staining Assay of KIR2DS2–HLA-A*11:01 Binding in Live Cells. To demonstrate whether KIR2DS2–HLA-A*11:01 binding occurs in live cells, KIR2DS2 tetramers were generated (*SI Materials and Methods*). The lymphoblastoid cell line BM03, homozygous for HLA-A11, was first tested to confirm expression of surface HLA-A11 using an A11-specific antibody (4i93; Abcam), whereas MF2, an HLA-A11–null cell line, and the MHC class I mutant 721.221 were both negative for HLA-A11 expression (Fig. S4 *A*–*C*). Using KIR2DS2 tetramers, BM03 showed strong staining when pulsed with 250 μg of the MLIYSMWGK peptide (WGK; Fig. S4*D*), whereas MF2 and 721.221 remained negative in the presence of the peptide as well as three other peptide variants, MLIYSMWAK (WAK), MLIYSMWSK (WSK), and MLIYSMWVK (WVK) (Fig. S4 *E* and *F*). Because tetramer staining is highly sensitive, it can be used to assess the impact of peptide on KIR–HLA binding. To do so, peptides with different side-chain volume residues at

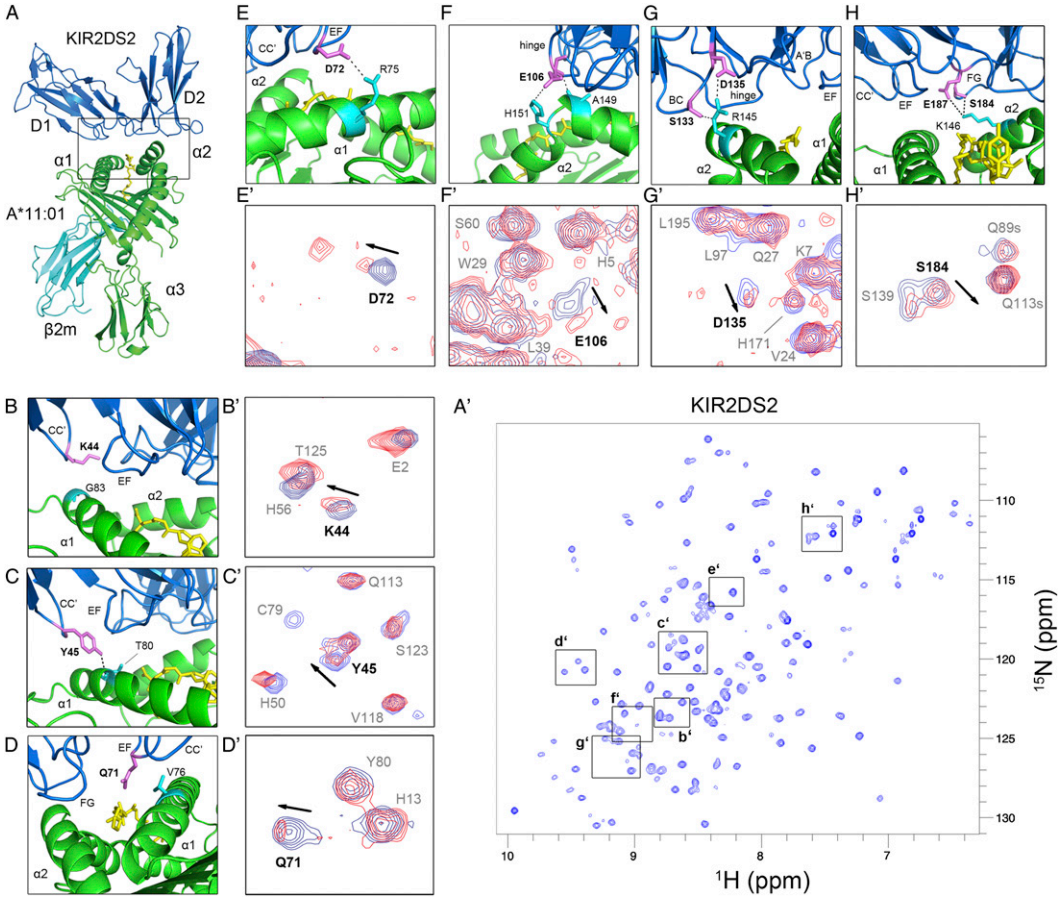

Fig. 3. Essential contact residues mapped by crystal structure and NMR chemical shift perturbation. (*A*) Overall view of the KIR–HLA complex with the contact interface highlighted in the black box. (*B*–*D*) Close-up views of K44, Y45, and Q71 (stick, violet). The adjacent residues on the α1-helix are highlighted (stick, cyan). (*E*–*H*) Close-up views of D72, E106, S133/D135, and S184. The adjacent residues on both helices are highlighted. Hydrogen bonds are shown as black dashed lines. (*A′*) Two-dimensional [^{1}H-^{15}N]-TROSY-HSQC spectrum of free KIR2DS2 recorded on an 800-MHz magnet. Relative positions of amino acids for detailed view are boxed. (*B′*–*H′*) Overlays of 2D [^{1}H-^{15}N]-TROSY-HSQC spectra of free KIR2DS2 (blue contours) and KIR2DS2 titrated with HLA-A*11:01 (red contours; KIR:HLA ratio, 1:3). The tracings of chemical shift change are indicated by arrows.

p8, Gly, Ser, Ala, Thr, Val, and Trp, as well as those with charged residues, Asp, Glu, Lys, and Arg, were synthesized. Interestingly, the replacement of Gly with Ser, Ala, Thr, Val, or Trp at the p8 position still permits the association between KIR2DS2 and HLA-A*11:01 (Fig. S4*G*). However, the presence of charged residues at p8 of the peptide uniformly resulted in loss of binding (Fig. S4*H*). In addition to the peptide sequence, binding is also influenced in a peptide dose-dependent manner (Fig. S4 *I*–*N*). Taken together, the cell-based tetramer binding assays demonstrate that KIR–HLA binding is not entirely peptide-agnostic.

Mutational Analysis of KIR2DS2-Binding Contact Residues. Using a surface plasmon resonance (SPR) assay, the binding interaction between KIR2DS2 and A*11:01 was first determined in triplicate, showing a K_D of ∼22 μM (Fig. 4 *A* and *C*–*F*). HLA-C controls C*08:01, and C*12:02 confirmed the lack of interaction between KIR2DS2 and HLA-C molecules (Fig. S5 *A* and *B*). Mutational analysis was carried out on all important contact residues of KIR2DS2 to verify their roles in providing stability to the KIR–HLA complex (Fig. 4 *A*, *B*, and *G*–*P*). Alanine mutants at positions 45, 71, 72, 104, 106, 135, 184, and 187 abrogated KIR–HLA binding, which confirmed the observations with inhibitory KIRs that a single amino acid change at a critical position can completely disrupt binding. An A11-binding motif (21, 22) comprising Pro71/Val72 was previously reported, and this was tested with a double mutation that changed Gln71/Asp72 of KIR2DS2 to Pro71/Val72. However, this did not result in any binding, which suggests that the Pro71/Val72 combination could function in the context of KIR2DS4 or KIR3DL2 but not necessarily in other KIRs such as KIR2DS2.

The mutants Lys44Ala, Tyr134Ala, and Tyr45Phe resulted in some loss of measurable binding, but this was insufficient to disrupt the overall stability of the KIR–HLA complex, which suggests that such disruption is compensated by the network of salt bridges and other hydrogen bonds that keep the binding intact. However, a Tyr45Ala mutation abrogated binding, suggesting that Ala is a more drastic change at this position than Phe, which is of the same aromatic amino acid grouping as Tyr (Fig. 4 *A*, *M*, and *N*). Hence, position 45 appears to be important to maintain the stability of KIR2DS2–HLA-A*11:01 binding given that alanine mutation abrogated binding whereas a similar mutation at the adjacent position 44 did not. The binding experiments were performed with both A*11:01 and A*11:02, which differ only at one amino acid (Glu19Lys), and both HLA alleles showed similar binding behavior to KIR2DS2. A*11:02 therefore provided a functional and validating replicate for the SPR binding studies.

Discussion

The main HLA ligand specificities for inhibitory KIRs are HLA-C (23, 24); however, the activating KIR2DS2 does not bind well to HLA-C. Although these observations have not been formally

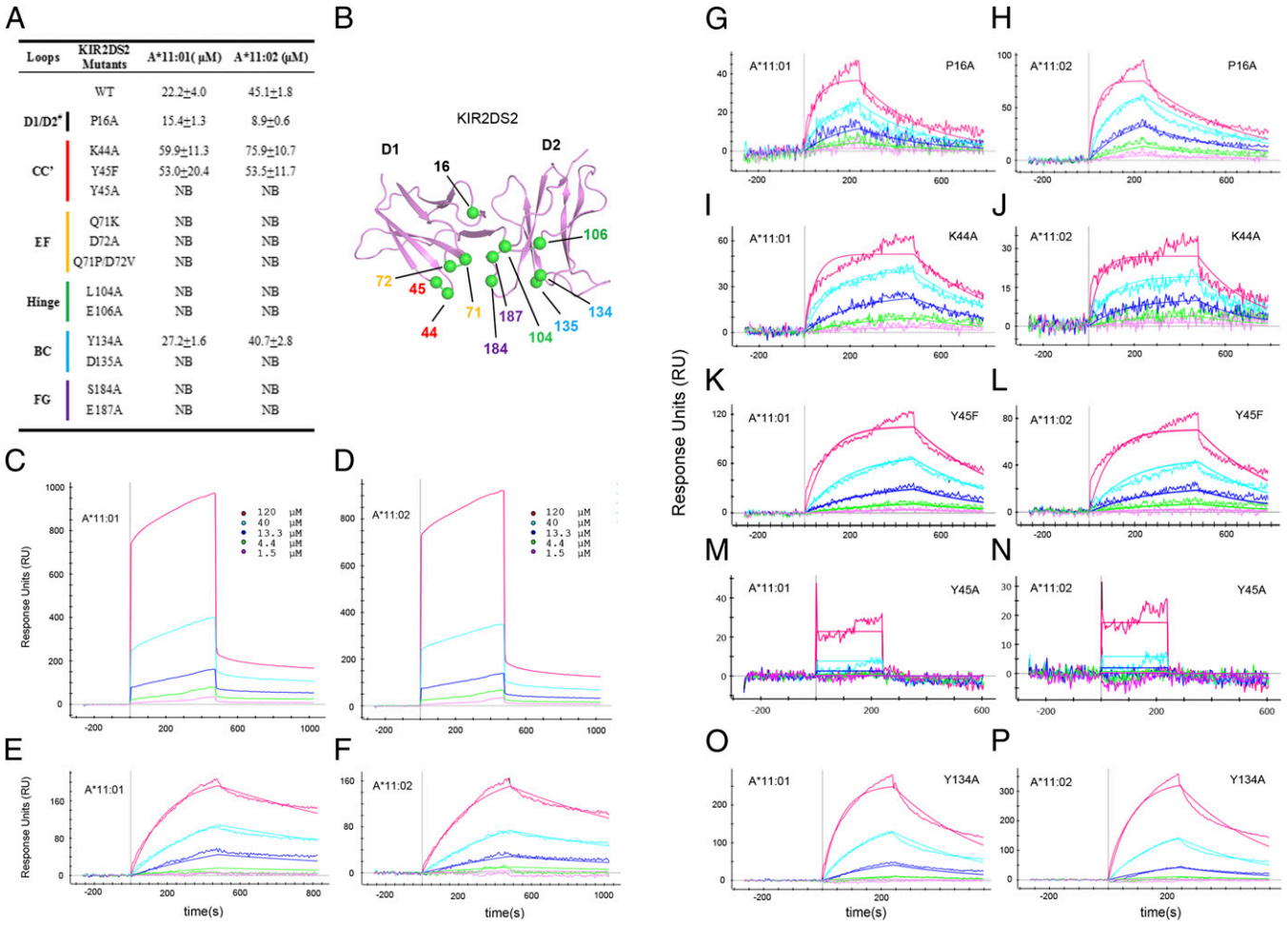

Loops	KIR2DS2 Mutants	A*11:01(μM)	A*11:02 (μM)
	WT	22.2±4.0	45.1±1.8
D1/D2*	P16A	15.4±1.3	8.9±0.6
CC′	K44A	59.9±11.3	75.9±10.7
	Y45F	53.0±20.4	53.5±11.7
	Y45A	NB	NB
EF	Q71K	NB	NB
	D72A	NB	NB
	Q71P/D72V	NB	NB
Hinge	L104A	NB	NB
	E106A	NB	NB
BC	Y134A	27.2±1.6	40.7±2.8
	D135A	NB	NB
FG	S184A	NB	NB
	E187A	NB	NB

Fig. 4. Effect of KIR2DS2 contact residue mutations on its binding to HLA-A*11 measured by SPR. SPR measurements were conducted to determine KIR–HLA binding affinities with the fitting model according to the Langmuir method (25). (*A*) Site-directed mutagenesis of specific amino acids was separately generated for KIR2DS2: P16A, K44A, Y45F, Y45A, Q71K, D72A, L104A, E106A, Y134A, D135A, S184A, and E187A were single mutants, whereas Q71P/D72V was a double mutant. Each interaction was assayed in at least two independent experiments, whereas the WT was tested in four independent experiments. Mean K_D values are given as μM with corresponding SDs. D1/D2#, KIR D1/D2 domain interface; NB, no binding. (*B*) The mutation positions in the CC′, EF, BC, and FG loops and hinge are colored in red, yellow, light blue, purple, and green, respectively. (*C* and *D*) SPR traces for WT KIR2DS2–A*11:01 and KIR2DS2–A*11:02. (*E* and *F*) Fitting curves for WT KIR2DS2–A*11:01 and KIR2DS2–A*11:02. This was generated by subtracting the control signals from *C* and *D*, respectively. (*G* and *H*) Fitting curves for the binding of KIR2DS2 (P16A)–A*11:01 and –A*11:02. (*I* and *J*) Fitting curves for the binding of KIR2DS2 (K44A)–A*11:01 and –A*11:02. (*K* and *L*) Fitting curves for the binding of KIR2DS2 (Y45F)–A*11:01 and –A*11:02. (*M* and *N*) Fitting curves for the binding of KIR2DS2 (Y45A)–A*11:01 and –A*11:02. (*O* and *P*) Fitting curves for the binding of KIR2DS2 (Y134A)–A*11:01 and –A*11:02.

proven using crystal structure data, amino acid substitution experiments have shown that replacement of tyrosine at position 45 alone of KIR2DS2 can restore some degree of binding activity with HLA-C. Although tantalizing, these results do not explain the mechanism behind the loss of binding with HLA-C and which specific residues of HLA are likely to engage with position 45 of KIR2DS2. In this study, we provide structural evidence that the activating KIR2DS2 binds to a previously unrecognized HLA ligand, A*11:01. In addition, the use of NMR and HSQC titration provides further confirmation of binding interactions by tracing chemical shift changes of specific residues.

In contrast with inhibitory KIRs, the role of position 44 in the activating KIR2DS2 is greatly diminished. The lack of significant binding interaction of position 44 is a major departure from its known function in inhibitory KIRs, and SPR data show that substitution of Lys44 with Ala does not result in a significant decline in binding. Of interest is position 45, which is a residue unique to KIR2DS2, and because no prior evidence has been shown that Tyr45 has a specific function, it has been speculated to constitute a "fatal" mutation (17) and that it has been actively selected to lose binding with HLA class I (8, 16). We found that Tyr45 has an important role in forming hydrogen bonds with the backbone of Thr80 of HLA. It does so by being positioned closer to the C terminus of the α1-helix, whereas in inhibitory KIRs, Phe45 is accommodated by the helix groove comprising the HLA-A*11:01 75–80 fragment through hydrophobic contacts. Mutating Tyr45 to Phe45 resulted in some loss of binding but was not abrogated completely, whereas an Ala45 mutant showed no binding. This suggests that position 45 plays an important role in maintaining the stability of the KIR2DS2–HLA-A*11:01 interaction.

The KIR2DS2–HLA-A*11:01 structure has revealed binding interactions that differ from those seen in inhibitory KIRs; these are the salt bridges Asp72-Arg75 and Glu187-Lys146, hydrogen bond Tyr45-Thr80, and hydrophobic interactions Tyr134-A149. Interestingly, KIR2DS4 has previously been shown to exhibit A*11:01 and A*11:02 binding specificity by means of a Pro71/Val72 motif at the D1 domain (22). Human KIR2DS4 shares this Pro71/Val72 motif with KIR3DL2, and is believed to have arisen

through a gene conversion event between the ancestral lineages of these two genes. KIR2DS4-Fc fusion proteins have shown binding to A*11:02 and to a lesser extent A*11:01, but the interacting residues between KIR and HLA have also not been formally proven. In KIR2DS2, Asp72 does not follow the binding interactions proposed for Val72 binding to KIR2DS4, because substitution of Asp72 with Val results in a loss of binding. Nevertheless, KIR2DS2 and KIR2DS4 have many residue differences such that Val72 may be relevant only to KIR2DS4. Our data show, however, that position 72 is an important residue (more so than position 44), and may be a binding paradigm for activating KIRs. Gln71 in KIR2DS2 does not participate in strong bond formation as with Asp72, but it is sufficiently close to being able to interact with p8 of the peptide. It appears that in inhibitory KIRs (26–28), bulky or strongly charged residues are likely to affect the overall KIR–HLA interaction.

In this study, the availability of structural information, live-cell tetramer staining, NMR, and SPR binding data together provides insight into the binding of activating KIR2DS2 to HLA-A*11:01 as its cognate ligand. Furthermore, the role of peptide sequence is demonstrated by altered KIR2DS2–tetramer binding when the peptide p8 residues are charged residues, and therefore lends understanding to how minimal amino acid changes can dramatically alter binding characteristics of highly homologous inhibitory KIRs. The identification of the unique network of critical residues in determining the binding specificity of activating KIRs and the mediation of peptide in KIR–HLA association will be the basis for future work on how KIRs are activated and their mechanism of action.

Materials and Methods

Full details of the methods are described in *SI Materials and Methods*. Briefly, single-wavelength native data of the KIR2DS2–HLA-A*11:01 crystal were collected with space group $P2_12_12_1$ with unit cell parameters a = 69.5, b = 94.7, c = 228.4, $\alpha = \beta = \gamma = 90°$ and further processed using CCP4 (29). Rigid-body and restrained refinement were performed using REFMAC5 (30). Model geometry of the complex was verified with PROCHECK (31), and PDBePISA (32) was used to generate interface data. The structure coordinates have been deposited in the Protein Data Bank under PDB ID code 4N8V.

ACKNOWLEDGMENTS. We thank Dr. Xue Bo [Institute of Molecular and Cell Biology, Agency for Science, Technology and Research (A*STAR)] for data collection at beamline BL13B1 of the National Synchrotron Radiation Research Center, Taiwan, and Jeffrey Pelton for 3D TROSY experiment acquisition at the Central California NMR Facility, University of California, Berkeley. We also thank Ester Khin for assistance in 2DS2 expression and purification and Dr. Evan Newell for advice on tetramer preparation and the staining assay. This work is funded by the Singapore Immunology Network, A*STAR.

1. Parham P, Moffett A (2013) Variable NK cell receptors and their MHC class I ligands in immunity, reproduction and human evolution. *Nat Rev Immunol* 13(2):133–144.
2. Vivier E, et al. (2011) Innate or adaptive immunity? The example of natural killer cells. *Science* 331(6013):44–49.
3. Lanier LL (2005) NK cell recognition. *Annu Rev Immunol* 23:225–274.
4. Fan QR, et al. (1997) Structure of the inhibitory receptor for human natural killer cells resembles haematopoietic receptors. *Nature* 389(6646):96–100.
5. Snyder GA, Brooks AG, Sun PD (1999) Crystal structure of the HLA-Cw3 allotype-specific killer cell inhibitory receptor KIR2DL2. *Proc Natl Acad Sci USA* 96(7):3864–3869.
6. Parham P, Norman PJ, Abi-Rached L, Guethlein LA (2012) Human-specific evolution of killer cell immunoglobulin-like receptor recognition of major histocompatibility complex class I molecules. *Philos Trans R Soc Lond B Biol Sci* 367(1590):800–811.
7. Joyce MG, Sun PD (2011) The structural basis of ligand recognition by natural killer cell receptors. *J Biomed Biotechnol* 2011:203628.
8. Moesta AK, et al. (2010) Humans differ from other hominids in lacking an activating NK cell receptor that recognizes the C1 epitope of MHC class I. *J Immunol* 185(7): 4233–4237.
9. Moesta AK, Parham P (2012) Diverse functionality among human NK cell receptors for the C1 epitope of HLA-C: KIR2DS2, KIR2DL2, and KIR2DL3. *Front Immunol* 3:336.
10. Fan QR, Long EO, Wiley DC (2001) Crystal structure of the human natural killer cell inhibitory receptor KIR2DL1-HLA-Cw4 complex. *Nat Immunol* 2(5):452–460.
11. Boyington JC, Motyka SA, Schuck P, Brooks AG, Sun PD (2000) Crystal structure of an NK cell immunoglobulin-like receptor in complex with its class I MHC ligand. *Nature* 405(6786):537–543.
12. Vivian JP, et al. (2011) Killer cell immunoglobulin-like receptor 3DL1-mediated recognition of human leukocyte antigen B. *Nature* 479(7373):401–405.
13. Béziat V, et al. (2013) NK cell responses to cytomegalovirus infection lead to stable imprints in the human KIR repertoire and involve activating KIRs. *Blood* 121(14): 2678–2688.
14. Askar M, et al. (2009) Lack of killer immunoglobulin-like receptor 2DS2 (KIR2DS2) and KIR2DL2 is associated with poor responses to therapy of recurrent hepatitis C virus in liver transplant recipients. *Liver Transpl* 15(11):1557–1563.
15. Jones DC, et al. (2006) Killer Ig-like receptor (KIR) genotype and HLA ligand combinations in ulcerative colitis susceptibility. *Genes Immun* 7(7):576–582.
16. Winter CC, Gumperz JE, Parham P, Long EO, Wagtmann N (1998) Direct binding and functional transfer of NK cell inhibitory receptors reveal novel patterns of HLA-C allotype recognition. *J Immunol* 161(2):571–577.
17. Older Aguilar AM, Guethlein LA, Abi-Rached L, Parham P (2011) Natural variation at position 45 in the D1 domain of lineage III killer cell immunoglobulin-like receptors (KIR) has major effects on the avidity and specificity for MHC class I. *Immunogenetics* 63(8):543–547.
18. Garboczi DN, Hung DT, Wiley DC (1992) HLA-A2-peptide complexes: Refolding and crystallization of molecules expressed in *Escherichia coli* and complexed with single antigenic peptides. *Proc Natl Acad Sci USA* 89(8):3429–3433.
19. Saulquin X, Gastinel LN, Vivier E (2003) Crystal structure of the human natural killer cell activating receptor KIR2DS2 (CD158j). *J Exp Med* 197(7):933–938.
20. Winter CC, Long EO (1997) A single amino acid in the p58 killer cell inhibitory receptor controls the ability of natural killer cells to discriminate between the two groups of HLA-C allotypes. *J Immunol* 158(9):4026–4028.
21. Pende D, et al. (1996) The natural killer cell receptor specific for HLA-A allotypes: A novel member of the p58/p70 family of inhibitory receptors that is characterized by three immunoglobulin-like domains and is expressed as a 140-kD disulphide-linked dimer. *J Exp Med* 184(2):505–518.
22. Graef T, et al. (2009) KIR2DS4 is a product of gene conversion with KIR3DL2 that introduced specificity for HLA-A*11 while diminishing avidity for HLA-C. *J Exp Med* 206(11):2557–2572.
23. Parham P (2005) MHC class I molecules and KIRs in human history, health and survival. *Nat Rev Immunol* 5(3):201–214.
24. Biassoni R, Ugolotti E, De Maria A (2009) NK cell receptors and their interactions with MHC. *Curr Pharm Des* 15(28):3301–3310.
25. Adamson AW, Gast AP (1999) *Physical Chemistry of Surfaces* (Wiley, New York), 6th Ed.
26. Malnati MS, et al. (1995) Peptide specificity in the recognition of MHC class I by natural killer cell clones. *Science* 267(5200):1016–1018.
27. Peruzzi M, Parker KC, Long EO, Malnati MS (1996) Peptide sequence requirements for the recognition of HLA-B*2705 by specific natural killer cells. *J Immunol* 157(8):3350–3356.
28. Rajagopalan S, Long EO (1997) The direct binding of a p58 killer cell inhibitory receptor to human histocompatibility leukocyte antigen (HLA)-Cw4 exhibits peptide selectivity. *J Exp Med* 185(8):1523–1528.
29. Winn MD, et al. (2011) Overview of the CCP4 suite and current developments. *Acta Crystallogr D Biol Crystallogr* 67(Pt 4):235–242.
30. Murshudov GN, Vagin AA, Dodson EJ (1997) Refinement of macromolecular structures by the maximum-likelihood method. *Acta Crystallogr D Biol Crystallogr* 53(Pt 3): 240–255.
31. Laskowski RA, Moss DS, Thornton JM (1993) Main-chain bond lengths and bond angles in protein structures. *J Mol Biol* 231(4):1049–1067.
32. Krissinel E, Henrick K (2007) Inference of macromolecular assemblies from crystalline state. *J Mol Biol* 372(3):774–797.